Thin Solid Films 685 (2019) 131–135

Contents lists available at ScienceDirect

Thin Solid Films

journal homepage: www.elsevier.com/locate/tsf

Multifunctional metal oxide electrodes: Colour for thin film solar cells

Nils Neugebohrn*, Kai Gehrke, Karoline Brucke, Maximilian Götz, Martin Vehse

DLR Institute of Networked Energy Systems, Urban and Residential Technologies, Carl-von-Ossietzky-Str. 15, 26129 Oldenburg, Germany

ARTICLE INFO

Keywords:
Building integrated photovoltaics
Copper indium gallium selenide
Oxide-metal-oxide structure
Coloured solar cells, front contact

ABSTRACT

Building integrated photovoltaics (BIPV) is an essential part to reduce the CO_2 footprint of metropolitan areas. Currently, full integration of photovoltaic elements in a building is a very costly and complex undertaking, as it usually requires expensive custom modules. In order to increase the market share of BIPV in the residential mass market, a low-cost, flexible technical process to change the appearance of solar elements is required. Transparent conductive electrodes consisting of an oxide-metal-oxide (OMO) stack of thin layers have been optimized for application in thin film solar cells. Here the OMO stack is multifunctional: It provides the transparent front contact electrode and at the same time allows tuning of the module colour. This has several advantages compared to other colouring techniques, i.e. coloured glass or additional interlayers. The OMO colouring does not require an additional process step, and with sputtering an already existing deposition method is used. By varying the thickness of the oxide layers it is possible to change the reflected spectrum of the stack and with it the module colour. In this publication, we present how the optical model of the OMO stack, that is necessary for precise tuning of the colour, is first developed for OMO/glass samples and then report the changes necessary to adapt the OMOs for use on Cu(In,Ga)Se2 thin film solar cells.

1. Introduction

The EU directive on the energy performance of buildings demands that by December 2020, all new buildings are nearly zero-energy [1]. Due to this legal requirement and other driving factors like economic advantages and the desire of companies for a greener image, the future cityscapes of Europe will include significantly more building integrated photovoltaics (BIPV) than currently. One challenge for the further growth of BIPV is locally varying building preferences and traditions. Often, expensively customized PV modules are required for full integration into each specific building project, which explains why BIPV is not as widespread as one might expect. A solution which includes both cost effective production and customization would be to separate both into a respective front and back end process: Standardized modules are mass produced at a competitive price and then distributed to local manufacturers, where they are finalized to custom modules. The application of an alternative front contact composite with included colour functionality for thin film solar cells discussed in this publication can be one step towards such a production concept.

A front contact for solar cells has to be both transparent and conductive. Transparent conductive oxides like aluminium-doped zinc oxide (AZO) and indium tin oxide (ITO) are typically used for this purpose [2–4]. The alternative transparent contact composite discussed here is an oxide-metal-oxide (OMO) multilayer stack. A thin metal layer is embedded between two oxide layers, implemented here with silver and AZO. The high conductivity of silver allows for the use a layer thickness of 6 to 12 nm, making it thin enough to allow a significant transmittance with a sheet resistance in the range of 3–10 Ω/sq. [5,6]. The oxide layers further reduce the reflection of the silver, especially in the visible range, which allows for the application of the OMO composite as a front contact in thin film solar cells (see Fig. 4). ITO and gallium doped zinc oxide function well for OMOs [5], but AZO is already typically in use for Cu(In,Ga)Se2 (CIGS) solar cell fabrication and an abundant material [4]. As the Ag layer provides the lateral conductivity of the OMO composite and the reflection is mainly determined by the oxide layers, it is to a certain degree possible to tune and optimize the conductivity and reflectivity separately, which is not the case for a standard AZO front contact. Nevertheless, a good electrical contact between the Ag layer and the remaining solar cell stack is still required from the AZO layer in between. The total thickness of an OMO optimized for transmittance in the visible range is about 100 nm. This enables together with the low deposition temperature fast deposition times compared to a standard AZO electrode. If the thickness of the oxide layers is increased, the reflection maximum of the OMO is shifted

* Corresponding author.
E-mail addresses: nils.neugebohrn@dlr.de (N. Neugebohrn), kai.gehrke@dlr.de (K. Gehrke), karoline.brucke@dlr.de (K. Brucke), maximilian.goetz@dlr.de (M. Götz), martin.vehse@dlr.de (M. Vehse).

https://doi.org/10.1016/j.tsf.2019.06.012
Received 20 November 2018; Received in revised form 10 May 2019; Accepted 7 June 2019
Available online 08 June 2019
0040-6090/

Table 1
Deposition parameters of sputtered Ag and AZO layers.

Process parameter	Ag	AZO
Gas flow Ar [sccm]	60	100
Gas flow O_2 [sccm]	0	0/5/10
Power [kW]	0.2	1
Pressure [Pa]	0.8	0.6
Distance target-substrate [mm]	70	75

into the visible range and thereby the colour appearance can be changed.

The OMO concept has been researched for several years, though previously more importance was attached to the application on flexible plastic substrates, e.g. organic luminescent displays or organic photovoltaic devices, which is possible due to the low deposition temperature of OMOs [5,6]. The use of OMO as coloured contact layers for a-Si:H cells has been demonstrated previously, and the topic has also found interest more recently [7–9]. In this work, we demonstrate the multifunctionality of the OMO composite as an electrode and as a colouring layer applied to CIGS cells, which compared to a-Si:H, is a more relevant and wide-spread technology, especially in the BIPV sector. We also show an optical simulation which was developed to allow for targeted design of colours CIGS cells.

2. Methods

OMO-composites were deposited via DC magnetron sputtering in a von Ardenne cluster tool type CS400PS with a 200 mm silver target and a 200 mm ZnO:Al target with 0.5 wt% Al_2O_3 doping. All OMOs were deposited at room temperature; further sputter parameters are given in Table 1. Two types of samples were used, which are displayed in Fig. 1. Microscope slides were used as glass substrates for the OMO-composites. Semi-finished, i.e. with a partial front contact, state of the art and Cd-free CIGS cells with a molybdenum back contact from AVANCIS were used for the application of an OMO-front contact on CIGS. The CIGS samples were cut to 2.5 × 2.5 cm^2, on which nine 0.25 cm^2 cells were structured by mechanical scribing. For encapsulation a polyvinyl butyral (PVB) lamination foil was used to attach the front glass. Current-voltage measurements were performed with a WACOM dual lamp solar simulator according to standard test conditions (AM1.5G-spectrum, 1000 W/m2, 25 °C). Reflection and transmission spectra were recorded with an UV-VIS Cary 5000 spectrophotometer with an integrating sphere. A Veeco Dektak 150 profilometer was used to determine layer thicknesses. Sheet resistances were measured with a Jandel RM3-AR.

One-dimensional optical simulations were performed with the software package SCOUT/CODE based on the transfer matrix method. The refractive indices n and k for AZO, Ag and PVB layers were generated from optical models provided by CODE, which were fitted to measured reflection and transmission spectra. For Ag, the susceptibility of free charge carriers is implemented with a Drude model in addition to a dielectric background. For AZO, in addition to the previous models, interband transitions are modelled with an optical -model describing the absorption in amorphous semiconductors by their electronic density of states based on a paper by O'Leary et al. [10], to which in the CODE-implementation a decay parameter is added. This allows the use of the Kramers-Kronig relation to compute the real part of the refractive index from the imaginary one. For encapsulation, the PVB was modelled with a combination of a Tauc-Lorentz model and four Kim oscillators [11,12]. For the remaining layers, mainly data from literature was used. The resulting simulated spectra are included in graphs of optical measurements throughout this work.

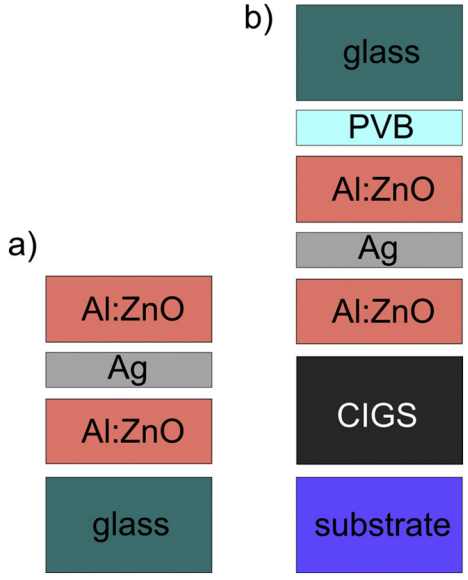

Fig. 1. Schematic drawing of the samples used in this study: OMO-composites consisting of a thin silver layer embedded between ZnO:Al layers were deposited on glass substrates (a) for optical characterization and on semi-finished CIGS cells (b). The CIGS samples were supplied by Avancis.

3. Results and discussion

3.1. OMO-composites on glass substrates

OMO-composites were deposited both on glass substrates and on semi-finished CIGS cells. To maximize the transmission of the OMO-composite, single layers were first optimized on glass substrates. In Fig. 2 AZO single layers of 300 nm thickness deposited with an oxygen flow of 0 and 10 sccm, respectively are shown. As can be seen, higher oxygen content leads to a higher transmission. For the sample deposited with an oxygen flow of 0 sccm, a sheet resistance of 781 ± 153 Ω/sq. was measured, while for the sample with 10sccm oxygen flow the sheet resistance was above the measurement range of 10 MΩ/sq. An increase in oxygen is known to decrease the amount of oxygen vacancies and carrier concentration in AZO [13], though as previously described, a high conductivity of AZO is not required in this case.

For Ag layers, the lowest thickness possible while retaining a high conductivity is optimal. As can be seen in Fig. 3, a thickness of at least 6 nm should be used, though a completely closed film seems to be only achieved for over 10 nm. For the application on solar cells, a thickness of 8 nm was chosen in order to account for detrimental effects of

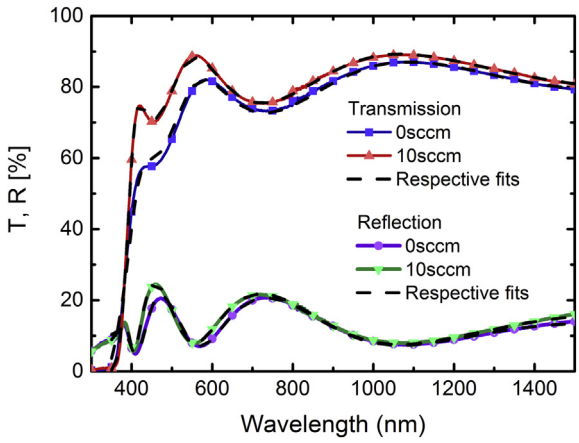

Fig. 2. Transmission and reflection of 300 nm AZO layers on glass substrates. Full lines are measurements; dashed lines are the output of the fitted optical models.

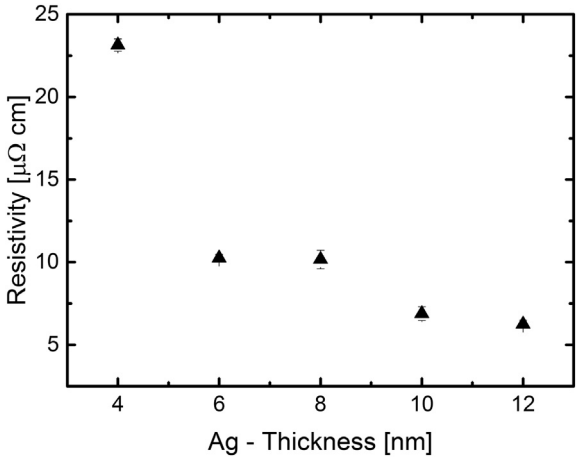

Fig. 3. Resistivity of Ag/glass samples. Below a critical thickness, the resistivity increases significantly.

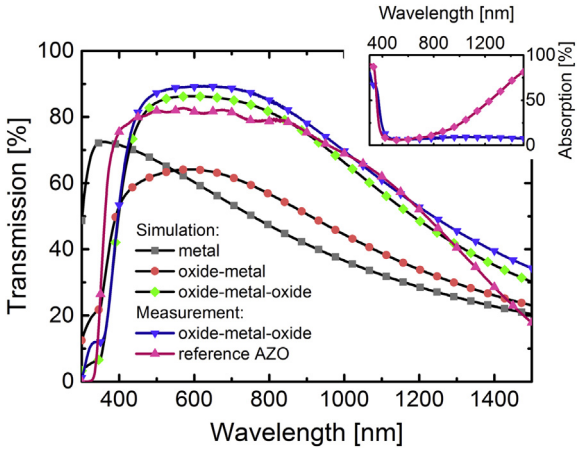

Fig. 4. Transmission spectra of OMO/glass compared to a commercial AZO/glass electrode. For the OMO, AZO layers with 52 nm thickness and 8 nm silver were used. Dashed lines indicate simulated transmission spectra of Ag/glass, AZO/Ag/glass and the complete OMO/glass. In the inset, absorption of OMO/glass and the reference electrode are shown.

roughness and different wettability of substrates. The transmission spectrum of an OMO stack on glass substrate is shown in Fig. 4 together with a commercially available front contact of roughly 900 nm AZO on glass. As can be seen, the OMO electrode performs similar or better than the reference electrode except for the wavelength range of 340–440 nm. This can be attributed to a further optimized AZO layer of the commercial electrode, which was usually also deposited at higher temperatures which leads to improved crystallinity and conductivity [4,14]. For the OMO/glass sample and the reference electrode sheet resistances of 8.4 ± 0.1 Ω/sq. and 7.8 ± 0.1 Ω/sq. respectively were measured. A sheet resistance of 5–10 Ω/sq. is typical for a CIGS front contact [4]. It follows that the OMO electrode on glass performs competitively.

It should be noted, that preliminary tests indicate that the exposure of the silver film to oxygen, e.g. due to the presence of oxygen gas during the deposition of subsequent layers, impacts the transmissivity of the OMO stack negatively, reducing the transmission by 3–4%. On the other hand, it is reported in literature, that an AgO_x layer of 1.5 nm can act as a beneficial wetting layer for thin silver layers [9]. However, as no sufficient reproducibility was reached for this result yet, it is not discussed further in this paper.

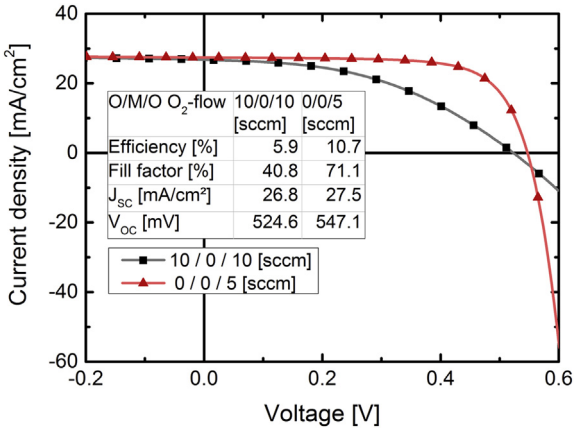

Fig. 5. Current density over voltage for OMO/CIGS cells with the bottom / top oxides deposited with O2 flows of 10/10 and 0/5 sccm and effciencies of 5.9% and 10.7% respectively. The layer thicknesses of both OMOs are 74/8/56 nm.

3.2. OMO-composites on CIGS solar cells

In order to transfer the OMO concept on CIGS solar cells, two additional aspects have to be considered: The OMO composite has to be electrically compatible with the solar cell, and, due to the change of optical environment, there is a shift in the reflected spectrum and colour. OMO-front contacts deposited with an O_2 flow of 10 sccm showed a reduced fill factor and an increased series resistance. The highest efficiency was obtained with the combination of 0 and 5 sccm O_2 flow for the bottom and upper AZO layer, respectively (see current-voltage curves in Fig. 5). This can be attributed to a to high resistivity of the bottom AZO layer for 10 sccm O_2, but as the layer in this case is only 74 nm thin, a better conduction band alignment related to a shift of the AZO work function at the interface of the OMO composite and the semi-finished CIGS cell for 0 sccm O_2 flow is also likely. Consequently, the following coloured OMO-composites were deposited with a combination of 0 scccm / 5 sccm O_2 flow for bottom / top oxide respectively. The shift in colour was achieved by increasing the thicknesses of the oxide layers (see Table 2) and the OMO-composites were deposited both on glass and CIGS.

In Fig. 6, the reflection spectra and photographs of three OMO/glass samples with varied colour are shown. With an increased thickness of the upper oxide layer, the reflection maxima are shifted to longer wavelength, though for the third, pink sample the reflection maximum of the next order already reaches the visible range.

In Fig. 7, photographs of the corresponding coloured OMO/CIGS samples together with the simulated colour are shown. The cells have an efficiency of 8–9%, compared to 15% for a cell with a standard AZO front contact. The cell parameters are summarized in Table 3. The efficiency is reduced by the current loss due to the light reflected for the coloured appearance, but further improvements should be possible as in the present development stage there are additional optical and electrical losses. Optically, both the semi-finished CIGS cell, as well as the encapsulation, needs to be considered. In comparison to the case of the same OMO on a glass substrate, a relatively small change in colour can be observed depending on both the specific OMO and characteristics of

Table 2
Thickness and oxygen flow for the layers of coloured OMO front contacts applied on glass and semi-finished CIGS cells. The values refer to the respective AZO/Ag/AZO layers (bottom to top).

Colour	Thickness [nm]	Oxygen flow [sccm]
Blue	175/8/217	0/0/5
Green	220/8/238	0/0/5
Pink, red	156/8/299	0/0/5

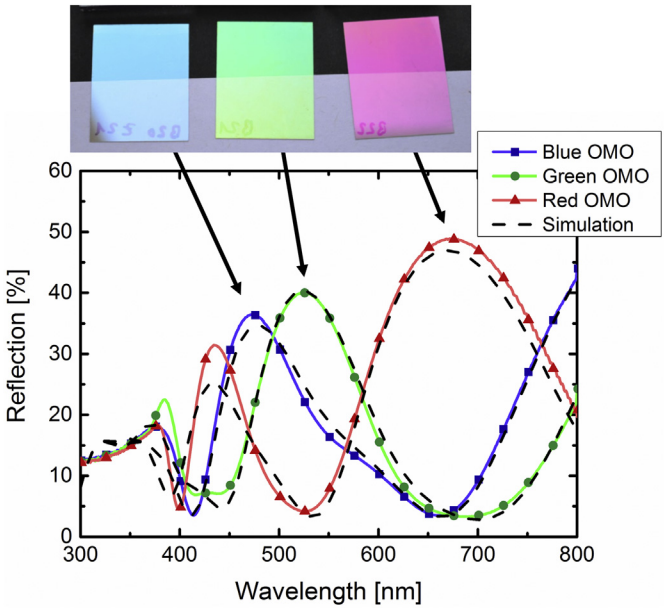

Fig. 6. Reflection spectra and photographs of coloured OMO/glass samples. Full lines are measurements, dashed lines are simulated spectra.

the top layer of the semi-finished CIGS cell. After encapsulation, a significant decrease in the intensity of the reflection was observed. The PVB foil for lamination and the front glass sheet have a refractive index of approximately 1.65 and 1.5 respectively, as is shown in Fig. 8. Therefore they act as an anti-reflective layer on top of the AZO layer with $n > 1.9$. In order to design coloured solar cells, the optical model was set up to include these layers.

In Fig. 9, the reflection spectrum of encapsulated OMO/CIGS cells is shown together with the simulation.

The simulated spectrum matches the measured adequately to allow targeted design of specific colours. The remaining mismatch stems from the challenges posed by high number of layers, and the roughness of the sample. Optically, the roughness also reduces the angle dependence of the colour appearance, as one sees always from a mixture of angles. Whether the colours of the encapsulated samples are clear enough or too muted remains to be tested with customers. Nevertheless we looked for ways to increase the reflection with our optical model. As shown in Fig. 10, according to the simulation the use of more layers, e.g. an OMOMO stack, is one option for clearer colours. Related experiments are currently in progress.

Table 3
Solar Cell Parameters. The values are taken from the best performing cell of a set of 9 present on each sample, except for the cell with the standard AZO front contact, for which the measurement values were provided by AVANCIS from a cell with standard AZO front contact prepared on the AVANCIS development line.

Type	Eff. [%]	J_{SC} [mA/cm^2]	V_{OC} [mV]	Fill factor [%]
OMO blue	8.1	20.9	556	69.6
OMO green	8.5	21.4	561	69.5
OMO red	8.2	21.5	552	69.0
Standard AZO	14.7	37.0	578	69.0

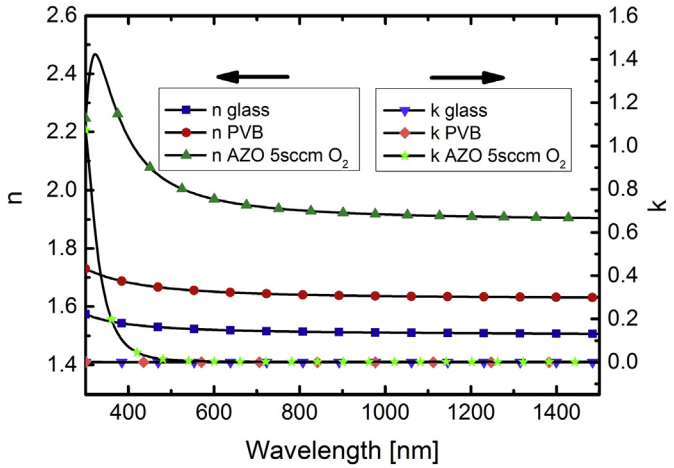

Fig. 8. Refractive indices n, k for AZO (deposited with 5sccm O2), PVB, and glass as used in the optical model. The data was generated from transmission and reflection spectra of single AZO/glass, glass/PVB/glass, and glass samples respectively.

4. Conclusion

In order to satisfy the need for affordable, customer-tailored BIPV panels, processes which allow for back end customization of standardized, semi-finished thin film modules are necessary. With this aim, the OMO-composite as an alternative front contact for thin film solar cells with added colour functionality was investigated. It could be demonstrated on glass substrates that the OMO front contact performs similar or better than a commercial reference AZO contact regarding sheet resistance and transmission. The colouring functionality was shown on glass substrates and on semi-finished CIGS cells in substrate configuration. Furthermore, an optimized oxygen content of the oxide layers

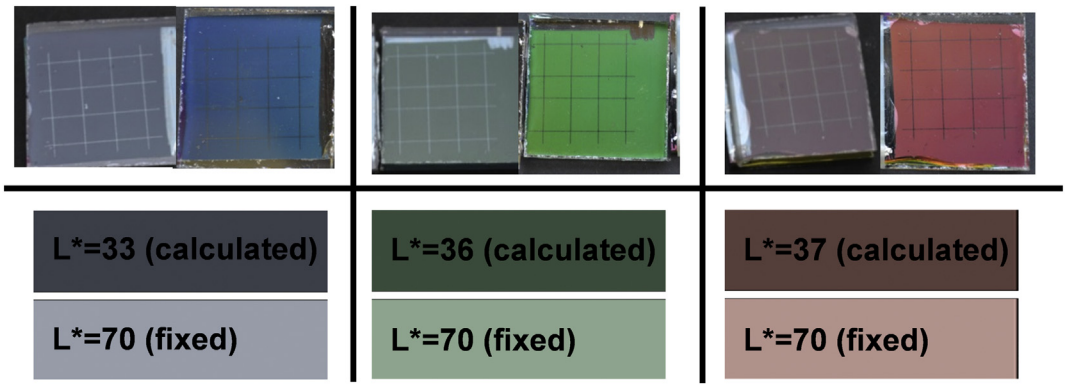

Fig. 7. Top: Photographs of blue, green and red encapsulated OMO/CIGS samples, as seen at a slight angle and from the top. Bottom: Colour as originally calculated by the optical model with illumination of a D65 (i.e., cloudy sky) spectrum, and with an increased lightness L*. (For interpretation of the references to colour in this figure legend, the reader is referred to the web version of this article.)

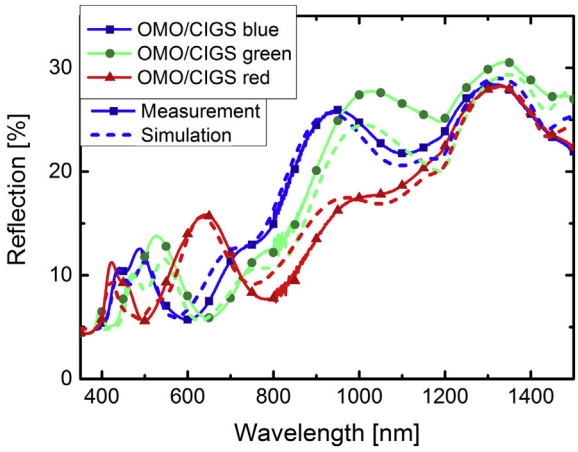

Fig. 9. Reflection spectra of blue, green and red OMO/CIGS cells. The measurements (full lines) are compared to the fit from the optical model (dashed lines). (For interpretation of the references to colour in this figure legend, the reader is referred to the web version of this article.)

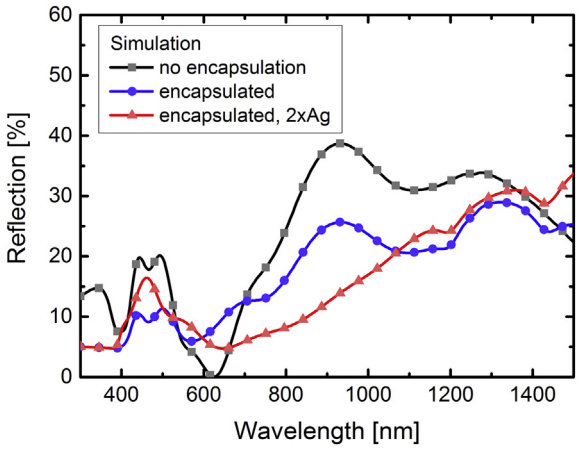

Fig. 10. Simulated reflection spectra of OMO/CIGS without encapsulation, with encapsulation and with encapsulation but with an OMOMO stack. The last case is one way to increase the strength of colours for encapsulated samples.

proved to be critical to the performance of OMO/CIGS cells. At the current stage, efficiencies of 8–9% could be achieved on CIGS with OMO-composites as colouring front contacts. The optical constants n, k for the layers of the OMO composite were generated from optical measurements and integrated in a simulation model based on the software SCOUT/CODE. The optical model was used for targeted design of colours. As the OMO-composite is deposited by sputtering at room temperature, it allows for the addition of colour in current production lines with existing technology. All colours can be produced flexible and just-in-time without the need to glue additional coloured foils or complicated logistics. With this process, we want to enable local manufacturers to finalize mass-produced semi-finished thin film modules to customer-tailored PV panels at a comparably low cost.

Acknowledgments

The authors gratefully acknowledge the funding of BMWi (FKZ 0324130A) in the German-Dutch ERANET collaboration project BIPVpod and AVANCIS GmbH for providing the CIGS samples used in this study and measurement values.

References

[1] Directive 2010/31/EU of the European Parliament and of the Council of 19 May 2010 on the energy performance of buildings (recast), Off. J. Eur. Union 18 (2010) 13–35.
[2] R. Mereu, S. Marchionna, A.L. Donne, L. Ciontea, S. Binetti, M. Acciarri, Optical and electrical studies of transparent conductive AZO and ITO sputtered thin films for CIGS photovoltaics, Phys. Status Solidi C 11 (2014) 1464–1467.
[3] M. Hála, S. Fujii, A. Redinger, Y. Inoue, G. Rey, M. Thevenin, V. Deprédurand, T.P. Weiss, T. Bertram, S. Siebentritt, Highly conductive ZnO films with high near infrared transparency, Prog. Photovolt. Res. Appl. 23 (2015) 1630–1641.
[4] R. Scheer, H.-W. Schock, Chalcogenide Photovoltaics: Physics, Technologies, and Thin Film Devices, John Wiley & Sons, 2011.
[5] C. Guillén, J. Herrero, TCO/metal/TCO structures for energy and flexible electronics, Thin Solid Films 520 (2011) 1–17, https://doi.org/10.1016/j.tsf.2011.06.091.
[6] M. Theuring, M. Vehse, K. von Maydell, C. Agert, AZO-Ag-AZO transparent electrode for amorphous silicon solar cells, Thin Solid Films 558 (2014) 294–297, https://doi.org/10.1016/j.tsf.2014.02.042.
[7] G. Kim, J.W. Lim, M. Shin, S.J. Yun, Bifacial color realization for a-Si: H solar cells using transparent multilayered electrodes, Sol. Energy 159 (2018) 465–474, https://doi.org/10.1016/j.solener.2017.11.019.
[8] J.W. Lim, G. Kim, M. Shin, S.J. Yun, Colored a-Si: H transparent solar cells employing ultrathin transparent multi-layered electrodes, Sol. Energy Mater. Sol. Cells 163 (2017) 164–169, https://doi.org/10.1016/j.solmat.2017.01.017.
[9] G. Zhao, W. Shen, E. Jeong, S.-G. Lee, S.M. Yu, T.-S. Bae, G.-H. Lee, S.Z. Han, J. Tang, E.-A. Choi, J. Yun, Ultrathin silver film electrodes with ultralow optical and electrical losses for flexible organic photovoltaics, ACS Appl. Mater. Interfaces 10 (2018) 27510–27520, https://doi.org/10.1021/acsami.8b08578.
[10] S.K. O'Leary, S. Johnson, P. Lim, The relationship between the distribution of electronic states and the optical absorption spectrum of an amorphous semiconductor: an empirical analysis, J. Appl. Phys. 82 (1997) 3334–3340, https://doi.org/10.1063/1.365643.
[11] C.C. Kim, J.W. Garland, H. Abad, P.M. Raccah, Modeling the optical dielectric function of semiconductors: extension of the critical-point parabolic-band approximation, Phys. Rev. B 45 (1992) 11749, , https://doi.org/10.1103/PhysRevB.45.11749.
[12] G. Jellison Jr., Spectroscopic ellipsometry data analysis: measured versus calculated quantities, Thin Solid Films 313 (1998) 33–39, https://doi.org/10.1016/S0040-6090(97)00765-7.
[13] S.-M. Park, T. Ikegami, K. Ebihara, P.-K. Shin, Structure and properties of transparent conductive doped ZnO films by pulsed laser deposition, Appl. Surf. Sci. 253 (2006) 1522–1527, https://doi.org/10.1016/j.apsusc.2006.02.046.
[14] J. Yoo, J. Lee, S. Kim, K. Yoon, I.J. Park, S. Dhungel, B. Karunagaran, D. Mangalaraj, J. Yi, High transmittance and low resistive ZnO: Al films for thin film solar cells, Thin Solid Films 480 (2005) 213–217, https://doi.org/10.1016/j.tsf.2004.11.010.